Resonance Reduction of Flexible Rotor with Hybrid Active Magnetic Bearings at Both Ends of the Shaft

Kento KATAOKA*, Satoshi UENO* and Chengyan ZHAO*
*Department of Mechanical Engineering, College of Science and Engineering, Ritsumeikan University
1-1-1 Noji-higashi, Kusatsu, Shiga 525-8577, Japan
E-mail: sueno@se.ritsumei.ac.jp

Abstract
This paper presents a hybrid active magnetic bearing (HAMB) system that uses both electromagnetic and permanent magnetic forces to support a flexible rotor. Unlike conventional active magnetic bearings, which require a bias current to generate bearing force, the proposed HAMB generates a bias magnetic flux using permanent magnets. This eliminates the need for a bias current and enabling reduced power consumption. The HAMB developed in this study exhibits negative stiffness in both the radial and tilt directions. Two HAMBs are installed at the ends of a horizontal flexible rotor to achieve magnetic levitation. To control levitation, a PD controller and an optimal controller based on the Linear Quadratic Regulator (LQR) method are employed. The LQR controller optimizes system performance while ensuring robustness against disturbances such as gravity-induced deflection and unbalanced forces during high-speed rotation. Sinusoidal disturbances were applied to the HAMB system, and the frequency responses in terms of rotor displacement and tilt were measured to model the resonance behavior of the elastic modes. Next, a motor was connected to one end of the rotor, and rotation tests were conducted. The results confirmed that the proposed LQR control allows stable passage through the critical speed associated with the first elastic mode. These two experiments demonstrate the effectiveness of the proposed control method in suppressing the resonance of the elastic modes.

Keywords : Magnetic bearings, Flexible rotor, Electromagnet, Permanent magnets, Liner quadratic regulator control

1. Introduction

A magnetic bearing is a mechanical component that uses magnetic forces generated by electromagnets (EMs) to support a shaft. The EMs are placed radially around the shaft, and controlling the current to the EMs maintains the shaft's position.

Recently, the design of rotating machinery, such as steam turbines and centrifugal compressors, has increased to include longer shafts and lighter weights in order to meet the current demand for higher rotational speeds. However, this trend inevitably leads to resonance causing rotational speeds to plateau. To address this issue, magnetic bearings, which use magnetic forces to levitate and support a rotor without physical contact, are being applied to industrial machinery. (The Institute of Electrical Engineers of Japan, 2018) Active magnetic bearings can provide damping for flexible mode resonances because the support force can be adjusted as needed.

This study focuses on supporting a flexible rotor with hybrid magnetic bearings (HAMBs), which use with two types of magnetic forces: permanent magnets (PMs) and electromagnets (EMs). (Ishikawa and Ueno, 2015) Since PMs generate the bias magnetic flux, no bias current is required, contributing to reduced power consumption. Additionally, the tilt moment of the magnetic bearing rotor can be controlled by shifting the center of gravity (COG) of the magnetic bearing rotor away from the point where the magnetic force is applied. (Ueno et al., 2024)

First, this paper describes the structure and principles of the HAMBs considered in the study and derives a model for the radial force and tilting moment. The study then investigates whether a flexible rotor using a fabricated HAMB, can safely pass critical speeds associated with bending modes. This evaluation determines the effectiveness of the proposed method.

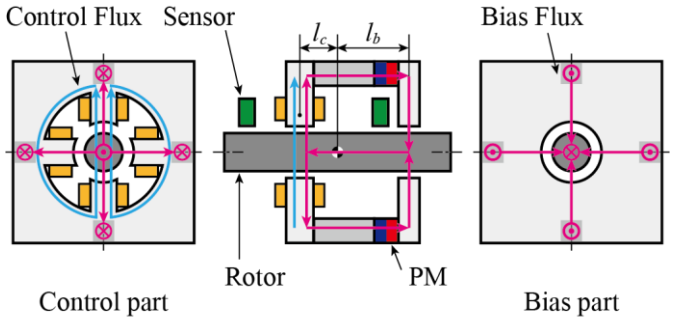

Fig. 1 Schematic drawing of HAMB.

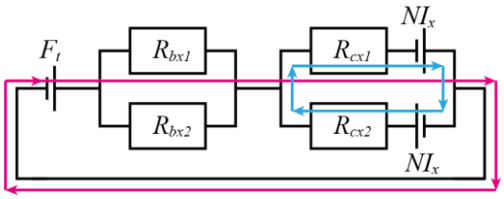

Fig. 2 Magnetic circuit for *x*-axis system.

2. Hybrid Active Magnetic Bearings

2.1 The structure and principles

Figure 1 illustrates the schematic structure and magnetic circuit of the HAMB used in this study. The HAMB consists of a control part with four salient poles and a bias section without salient poles. The parts are aligned in the axial direction and the distances from the COG are defined as l_c and l_b. The control and bias parts are connected via PMs and ferromagnetic materials, and forming a magnetic circuit between the rotor and stator.

All of the PMs are magnetized in the same direction. This produces a uniform radial bias flux in the air gaps of the control and bias parts. In the control part, control flux is generated by applying currents in opposite directions to the upper/lower or left/right coils. This increases the magnetic flux on one side of the air gap while decreasing it on the opposite side, thereby generating a radial force. Additionally, when the rotor is displaced, the magnetic reluctance decreases in the direction of displacement decreases, leading to an increase in magnetic flux. As a result, negative stiffness is produced in both the radial and tilting directions.

2.2 Modeling HAMB

The modeling of the HAMB is performed based on a conventional magnetic circuit approach. Figure 2 shows the magnetic circuit corresponding to one axis of the system. In the circuit, the total magnetomotive force (MMF) of the permanent magnets arranged in parallel is denoted by F_t. The nominal air gap when the target is centered in the HAMB is g_0, the permeability of free space is μ_0, the displacements of the bias and control parts are x_b and x_c and the cross-sectional areas are S_b and S_c respectively. The number of coil turns is N, and the control current in the x-direction is I_x. Let the displacement of the rotor center be *x*, and the tilt angle be θ. Considering that the magnetic reluctance of each section varies with the displacement of the target, the reluctances of each gap are defined as:

$$\begin{cases} R_{gbx1} = \frac{g_0 - x_b}{\mu_0 S_b} \\ R_{gbx2} = \frac{g_0 + x_b}{\mu_0 S_b} \\ R_{gcx1} = \frac{g_0 - x_c}{\mu_0 S_c} \\ R_{gcx2} = \frac{g_0 + x_c}{\mu_0 S_c} \end{cases} \tag{1}$$

where the subscripts 1 and 2 indicate components located in the positive and negative displacement directions, respectively, while the subscripts *b* and *c* indicate components belonging to the bias and control parts. Assuming small displacements, the positions are approximated as:

$$\begin{cases} x_b = x + l_b\theta \\ x_c = x - l_c\theta \end{cases} \tag{2}$$

Substituting Eq. (2) into Eq. (1), we get:

$$\begin{cases} R_{gbx1} = \frac{g_0 - x - l_b\theta}{\mu_0 S_b} \\ R_{gbx2} = \frac{g_0 + x + l_b\theta}{\mu_0 S_b} \\ R_{gcx1} = \frac{g_0 - x + l_c\theta}{\mu_0 S_b} \\ R_{gcx2} = \frac{g_0 + x - l_c\theta}{\mu_0 S_b} \end{cases} \tag{3}$$

Based on the superposition principle, applying Kirchhoff's law to each MMF source, the magnetic flux in each gap is expressed as:

$$\begin{cases} \Phi_{pb1} = \frac{\mu_0 S_b S_c H_t (g_0 + x + l_b\theta)}{(S_b + S_c) g_0^2 - S_c (x + l_b\theta)^2 - S_b (x - l_c\theta)^2} \\ \Phi_{pb2} = \frac{\mu_0 S_b S_c H_t (g_0 - x - l_b\theta)}{(S_b + S_c) g_0^2 - S_c (x + l_b\theta)^2 - S_b (x - l_c\theta)^2} \\ \Phi_{pc1} = \frac{\mu_0 S_b S_c H_t (g_0 + x - l_c\theta)}{(S_b + S_c) g_0^2 - S_c (x + l_b\theta)^2 - S_b (x - l_c\theta)^2} \\ \Phi_{pc2} = \frac{\mu_0 S_b S_c H_t (g_0 - x + l_c\theta)}{(S_b + S_c) g_0^2 - S_c (x + l_b\theta)^2 - S_b (x - l_c\theta)^2} \end{cases} \tag{4}$$

This study assumes that both the displacement and tilt angle of the rotor are sufficiently small. Therefore, the magnetic flux in each section is considered to vary linearly with displacement and tilt. Applying a Maclaurin expansion and taking only the first-order terms in Eq. (4), we obtain:

$$\begin{cases} \Phi_{pb1} \approx \alpha + \beta x + \beta l_b\theta \\ \Phi_{pb2} \approx \alpha - \beta x - \beta l_b\theta \\ \Phi_{pc1} \approx \alpha + \beta x - \beta l_b\theta \\ \Phi_{pc2} \approx \alpha - \beta x + \beta l_b\theta \end{cases} \tag{5}$$

where,

$$\alpha = \frac{\mu_0 S_b S_c H_t}{(S_b + S_c) g_0}, \qquad \beta = \frac{\mu_0 S_b S_c H_t}{(S_b + S_c) g_0^2}$$

Accordingly, the attractive magnetic force generated in each air gap can be expressed as:

$$F = \frac{\Phi^2}{\mu S} \tag{6}$$

Thus, the forces generated in each part are given by:

$$\begin{cases} F_{pb1} \approx \frac{1}{\mu S_b} (\gamma x + \gamma l_b\theta) \\ F_{pb2} \approx \frac{1}{\mu S_b} (-\gamma x - \gamma l_b\theta) \\ F_{pc1} \approx \frac{1}{\mu S_c} (\gamma x - \gamma l_b\theta) \\ F_{pc2} \approx \frac{1}{\mu S_c} (-\gamma x + \gamma l_b\theta) \end{cases} \tag{7}$$

where,

$$\gamma = \frac{(\mu_0 S_b S_c H_t)^2}{(S_b + S_c)^2 g_0^3}$$

Let F_b and F_c be the forces generated in the bias and control sections, respectively, from here,

$$\begin{cases} F_b = F_{pb1} - F_{pb2} = k_b x + k_b l_b\theta \\ F_c = F_{pc1} - F_{pc2} = k_c x + k_c l_c\theta \end{cases} \tag{8}$$

where the equivalent stiffnesses of the bias and control parts are:

$$k_b = \frac{(\mu_0 S_b S_c H_t)^2}{\mu S_b (S_b + S_c)^2 g_0^3}, \qquad k_c = \frac{(\mu_0 S_b S_c H_t)^2}{\mu S_c (S_b + S_c)^2 g_0^3}$$

Next, the force generated by the EMs is considered. As shown in Fig. 2, the MMF due to the electromagnets can be described as:

$$F_{EM} = NI_x \tag{9}$$

Using this, Kirchhoff's law yields the magnetic fluxes in the two air gaps as:

$$\Phi_{EMc1} = \Phi_{EMc2} = \frac{\mu_0 S_c N I_x}{2g_0} \tag{10}$$

From Eq. (6), the forces generated in each section are:

$$F_I = \frac{\mu_0 S_c (N I_x)^2}{4g_0^2} \tag{11}$$

In this study, the control current is assumed to be sufficiently small relative to the system scale, allowing the relationship between current and force to be considered linear. Thus, by linearizing Eq. (11), we obtain:

$$F_I = k_i I_x \tag{12}$$

where,

$$k_i = \frac{\mu_0 S_c N^2}{g_0^2}$$

Finally, based on Eq. (8) and Eq. (12), the radial force and torque about the center of mass of the rigid body can be described as:

$$\begin{bmatrix} F_x \\ M_y \end{bmatrix} = \begin{bmatrix} k_b + k_c & l_b k_b - l_c k_c \\ l_b k_b - l_c k_c & l_b^2 k_b + l_c^2 k_c \end{bmatrix} \begin{bmatrix} x \\ \theta \end{bmatrix} + \begin{bmatrix} k_i \\ -k_i l_c \end{bmatrix} I_x \tag{13}$$

It follows that both radial forces and tilting torques are generated due to rotor displacement, tilt, and the control current.

2.3 Experimental setup

The configuration of the experimental setup used in this study is shown in Fig. 3. The setup consists of a thin elastic rotor with a disk mounted at its center. The rotor is supported at both ends by the HAMB. Figure 4 shows a photograph of the fabricated HAMB. Each HAMB is equipped with four displacement sensors to measure the tilt angle of the rotor: two sensors in the horizontal direction and two in the vertical direction. The shaft diameter is 10 mm to induce elastic mode resonance at a relatively low frequency. The cylindrical sections of the rotor at both ends were designed with sufficient wall thickness to be treated as rigid bodies. In the hanging test, the natural frequencies of the rotor were measured to be 25Hz for the first elastic mode and 73Hz for the second.

2.4 Configuration of the control system

A digital signal processor (DSP; dSPACE: DS1103) was employed to implement the control system. The rotor's radial displacement was measured with an eddy current displacement sensor (SENTEC, LS-500). The analog signals were digitized via A/D converters and transmitted to the DSP. The DSP executed control computations in real time, and the output control signals were converted to analog voltages through a D/A converter. These voltages were then amplified using a power amplifier to drive current through the magnetic bearing coils.

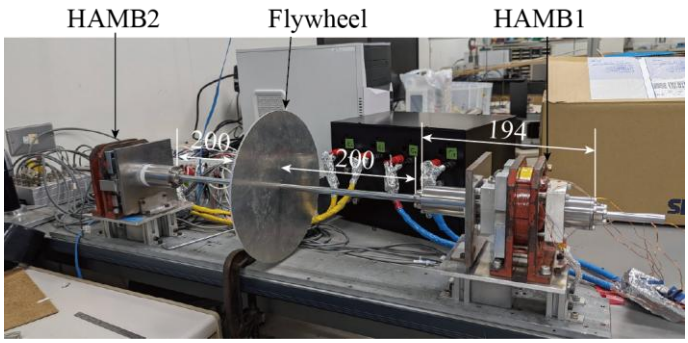

Fig. 3 Overview of experimental setup.

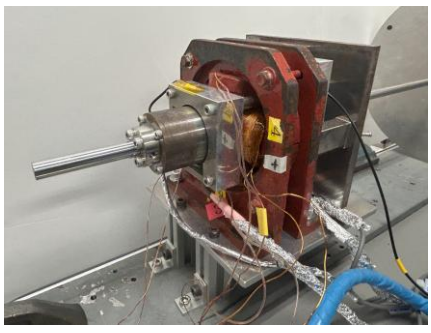

Fig. 4 Photograph of HAMB.

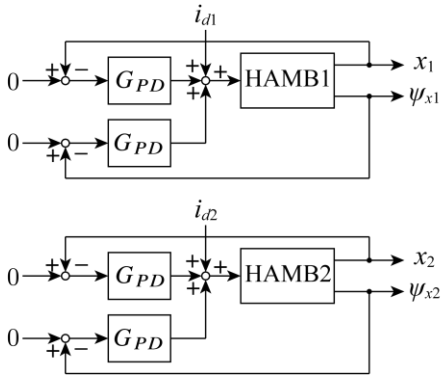

Fig. 5 Block diagram of PD controllers.

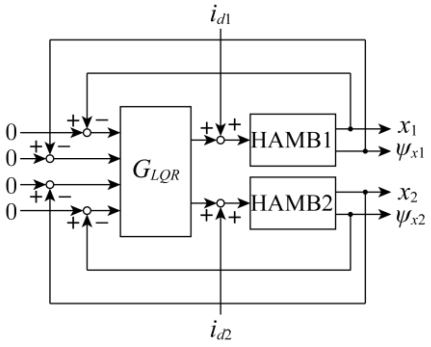

Fig. 6 Block diagram of LQR controller.

This study utilized two types of controllers: a PD controller and an optimal controller based on the Linear Quadratic Regulator (LQR) method. Figures 5 and 6 show the block diagrams of the PD and LQR controllers, respectively. The PD controller acts on both the displacement and tilt of the rotor. The LQR controller computes feedback gains by minimizing a quadratic cost function that includes weighting matrices Q and R, which assign relative importance to the state variables x and the control input u, respectively.

$$J = \int_0^\infty (x^T Q x + u^T R u) dt \tag{14}$$

The weighting matrices were carefully selected to appropriately reflect the control priority of each variable. To improve robustness against external disturbances and gravitational forces during steady-state levitation, an integral (I) control component was incorporated into the LQR framework. The controller design considered two major disturbances: rotor deflection due to gravitational loading, and shaft disturbances occurring during high-speed rotation, and was tuned to address both.

To compare control performance, experiments were conducted using both the PD and LQR controllers to regulate rotor displacement and tilt. The PD controller gains were derived by extracting the proportional and derivative components corresponding to displacement and velocity from the LQR gain matrix. The controller gain parameters for the x-axis direction of the PD and LQR controllers are shown in Tables 1 and 2, respectively.

Table 1 Gains of the PD controller.

	x_1	x_2	ψ_{x1}	ψ_{x2}
K_P	3044.4	3141.0	-21.8	16.6
K_D	18.0	20.2	-0.1	0.1

Table 2 Gains of the LQR controller.

	x_1	x_2	ψ_{x1}	ψ_{x2}	$\dot{x}_1$	$\dot{x}_2$	$\dot{\psi}_{x1}$	$\dot{\psi}_{x2}$
K_x	3044.4	159.3	-21.8	-15.8	18.0	1.0	-0.1	-0.1
	216.5	3141.0	18.2	16.5	1.2	20.2	0.12	0.1

3. Experimental Results

3.1 Frequency Response Test

Frequency response measurements were conducted to evaluate the frequency response characteristics of the HAMB levitation system. Figures 7 and 8 show the measured results. In each control condition, sinusoidal disturbances with an amplitude of ±0.05 [A] were applied to a stably levitated rotor via the inputs i_{d1} and i_{d2}, which were injected after the controller. The corresponding rotor displacements were then measured. Both figures present the results for HAMB1. After allowing sufficient time for the transient response to settle following the application of the disturbance, the gain

and phase were determined from the steady-state input and output waveforms.

Based on the measurement results, no significant difference in the displacement amplitude was observed between the two control methods. However, the LQR controller was clearly effective in the tilt direction. While the PD controller exhibited a prominent peak around 18 Hz in the tilt response, the LQR controller successfully suppressed this peak. Furthermore, the gain in tilt was reduced at approximately 66 Hz under LQR control, which further indicating the effectiveness of the proposed method. These results confirm that the LQR controller achieved improved bearing control performance.

The vibration modes can be inferred from the actual waveform data. Figures 9 and 10 show the displacement and tilt waveforms at approximately 18 Hz and 66 Hz, respectively. Figure 11 presents a predicted mode shape model of the flexible rotor. Based on this model, the mode near 18 Hz is identified as the first bending mode, and the mode near 66 Hz is identified as the second bending mode.

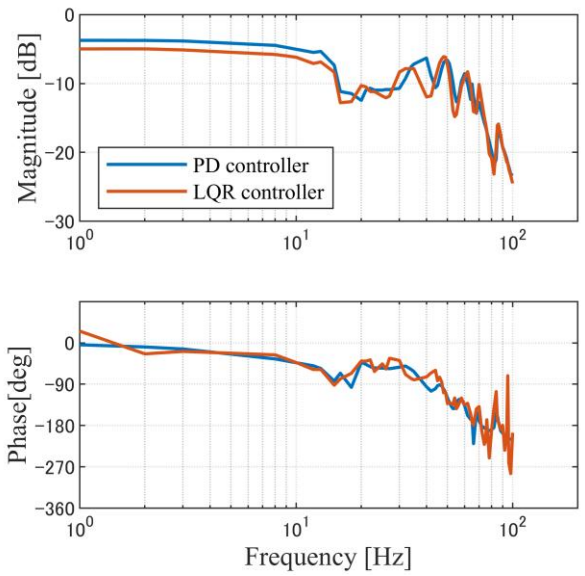

Fig. 7 Frequency response of displacement.

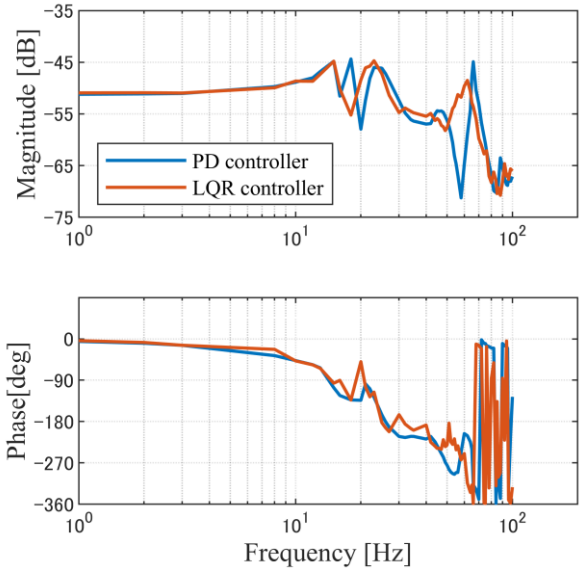

Fig. 8 Frequency response of tilt.

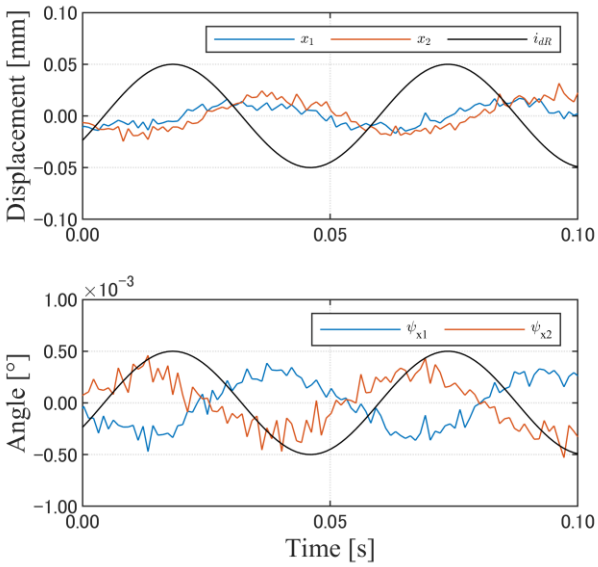

Fig. 9 Displacement and tilt under 18 Hz disturbance.

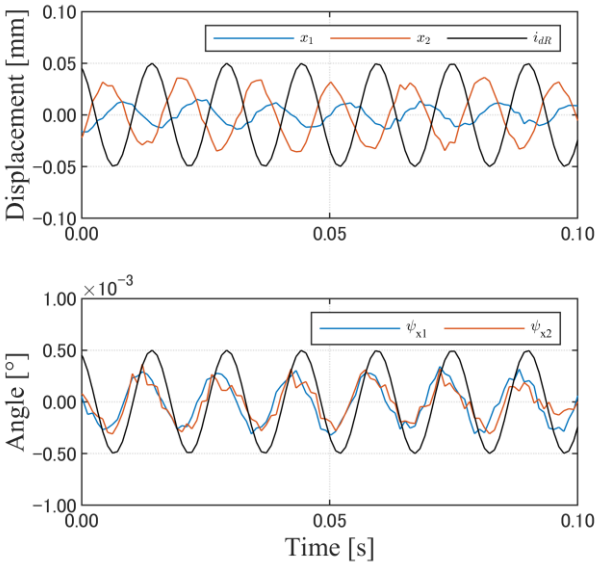

Fig. 10 Displacement and tilt under 66 Hz disturbance.

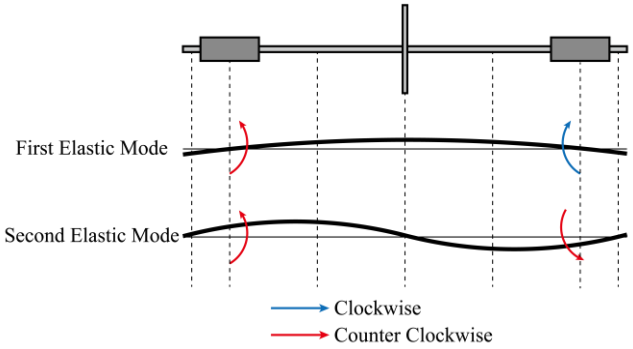

Fig. 11 Predicted mode shapes of the flexible rotor.

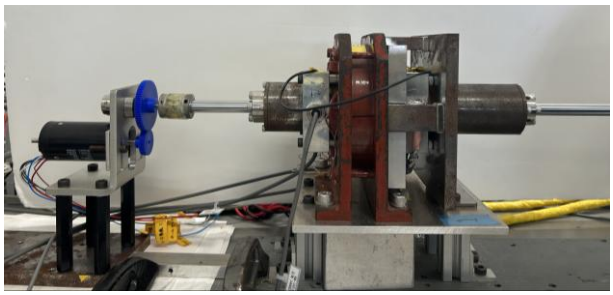

Fig. 12 Motor setup for rotation test.

3.2 Rotational Test

To evaluate the levitation and rotational characteristics of the system and verify the passage through resonance frequencies during rotation, levitated rotation tests were conducted. As shown in Fig. 12, the experiments were carried out with the rotor levitated, and a motor was mounted on the HAMB2 side. The rotational speed was increased from 0 to 40 Hz in 1 Hz increments, and the vibration amplitude of the rotor was measured after reaching steady-state rotation. In addition, finer measurements were performed near the resonance peaks identified in the frequency response tests.

Since the PD controller failed to maintain stable rotation despite achieving levitation, only the results obtained using the LQR controller are presented. The results of the Fast Fourier Transform (FFT) analysis of displacement and tilt in the x- and y-directions during rotation are shown in Figures 13 and 14, respectively. Both figures present the results for HAMB1.

According to the measurements, a vibration peak appeared around 18–20 Hz in the x-direction. However, the system successfully and stably passed through the critical speed associated with the first elastic mode. On the other hand, in the tilt results, both x- and y-directions exhibited increasing amplitudes beyond 40 Hz, leading to touchdown events as the rotational speed increased.

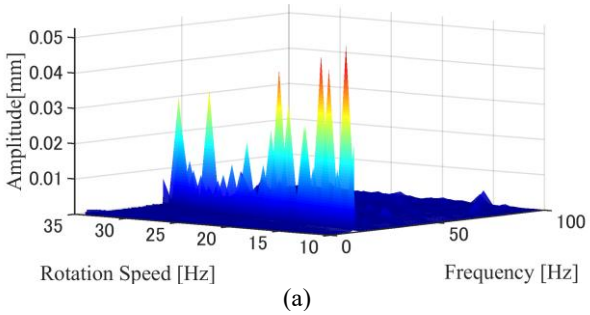

(a)

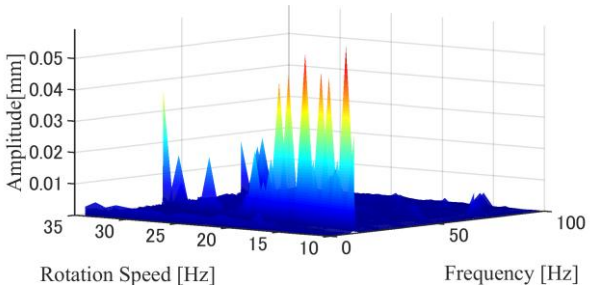

(b)

Fig. 13 FFT results of displacement:
(a) x-direction, (b) y-direction.

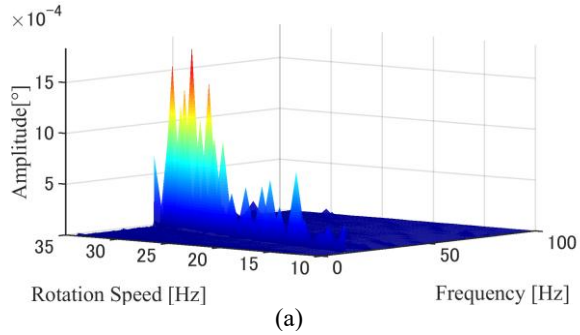

(a)

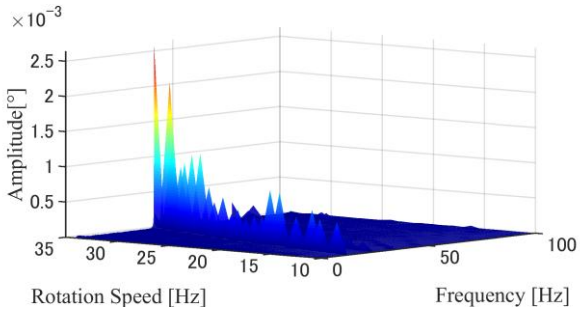

(b)

Fig. 14 FFT results of tilt:
(a) x-direction, (b) y-direction.

4. Conclusion

In this study, the HAMB with axially arranged control and bias magnetic circuits was used to support a flexible rotor, and the performance of two controllers was compared based on frequency response measurements. The results confirmed that, compared to the PD controller, the LQR controller was effective in suppressing resonance of the second elastic mode in the angular direction. Furthermore, in the rotation tests, the system was able to stably pass through the critical speed corresponding to the first elastic mode, demonstrating the effectiveness of the proposed method.

Future work will focus on optimizing the LQR gain to enable stable passage through the second elastic mode and further verify the effectiveness of the proposed control strategy.

References

Carlos, R. M., Mark, W. S., Eric, J. H., Electromagnetic Forces in a Hybrid Magnetic-Bearing Switched-Reluctance Motor, IEEE Transactions on Magnetics, Vol. 44, No. 12, (2008), pp.4626–4638

Ishikawa, N., Ueno, S., Levitation of a flexible rotor supported by hybrid magnetic bearings, Mechanical Engineering Journal, Vol. 2, No. 4 (2015)

Ito, M., Fujiwara, H., Matsushita, O., A Q-value Measurement for Damping Evaluation and Rotational Test of Over-Hung Rotor Supported by AMBs, Journal of the Japan Society of Mechanical Engineers, Vol.73, No.727 (2007), pp.21–28 (in Japanese).

Kanemitsu, Y., Takahashi, N., Fukushima, Y et al., Magnetic Bearing Guide for Rotating Machine Designers Book (in Japanese), Nippon Kogyo Publishing (2004).

Nagashima, T., This is the Finite Element Method (in Japanese), Shuwa System Co. (2015)

Okada, Y., Miyazawa, H., Kondo, R., Enokizono, M., Development of Flux Concentrated Hybrid Type Magnetic Bearings, Journal of the Japan Society of Mechanical Engineers, Vol.77, No.775 (2011), pp.302–311 (in Japanese).

Peter. K. B., Article to the Theory and Application of Magnetic Bearings, International Symposium on Power Electronics, Electrical Drives, Automation and Motion (2012), pp.1526–1534

Sagawa, K., Suzuki, E., Kondo, R., Okada, Y., Development and Application of Parallel PM Type Hybrid Magnetic Bearing, Journal of the Japan Society of Mechanical Engineers, Vol.73, No.733 (2007), pp.81–87 (in Japanese).

The Institute of Electrical Engineers of Japan, Magnetic Levitation Technology Research Committee, Principles and Applications of Magnetic Levitation Technology (in Japanese), Kagaku Joho Publishing (2018).

Ueno, S., Goto, K., Zhao, C., Control of a flexible rotor by hybrid active magnetic bearings using feedback of the tilt angle of the rotor, Proc. of 17th International Conference on Motion and Vibration & 20th Asia-Pacific Vibration Conference (2024)